Stability of $CaXe_3$ under Extreme Conditions

Pan Zhang(张盼)[1,3], Wei Yin(尹伟)[1,3], Yabin Ma(马亚斌)[1,3], Xuecong Pan(潘学聪)[1†], Shicong Ding(丁世聪)[2†], Jian Hao(郝健)[2], Jingming Shi(石景明)[2†] and Yinwei Li(李印威)[2]

[1]*School of Sciences, Xinjiang Institute of Technology, Aksu 843100, China*

[2] *Jiangsu Key Laboratory of Extreme Multi-Field Materials Physics, School of Physics and Electronic Engineering, Jiangsu Normal University, Xuzhou 221116, China*

[3]*Solid-State Physics and Quantum Precision Measurement Laboratory, Aksu 843100, China*

High pressure modifies the valence electron configuration of elements, enabling the formation of compounds with unconventional stoichiometries. In this work, we employ the CALYPSO structure search and density functional theory calculations to explore the structural phase transitions and electronic properties of calcium-xenon compounds under 170-290 GPa. Calculated formation enthalpies identify a Xe-rich $CaXe_3$ compound that adopts a tetragonal *P*4/*mmm* phase at 170 GPa and transforms to a monoclinic *C*2/*m* phase near 220 GPa. Electronic property calculations confirm that both phases are metallic. Ab initio molecular dynamics simulations indicate solid-like behavior at the sampled conditions between 170 and 290 GPa and at temperatures up to 9,000 K. The predicted stability range overlaps with pressure-temperature conditions expected in the deep interiors of rocky super-Earths, suggesting that $CaXe_3$ may serve as a potential Xe-bearing phase in such environments. These findings deepen our understanding of the high-pressure chemistry of inert-element-containing compounds and lay a theoretical foundation for discovering new alkaline earth metal-noble gas compounds.

Keywords: high pressure; Xenon-rich compounds; structure prediction; first-principles calculations

PACS: no more than four PACS codes should be provided

1. Introduction

Noble gases are generally regarded as chemically inert under ambient conditions owing to their closed-shell electronic configurations, which strongly suppress chemical reactivity and thereby make them unlikely to form stable compounds with other species. However, recent advances in theoretical and experimental high-pressure studies have significantly expanded our understanding of the physical and chemical behavior of noble gases.[1-3] Studies over the past few decades have shown that, under sufficiently high pressure, noble gases can display unexpected chemical reactivity and form thermodynamically stable compounds with metals,[4-9] closed-shell neutral molecules NH_3, CH_4, H_2O, SiO_2, CO_2, FeO_2,[10-22] and even other noble gases.[23-26] The associated interactions can vary widely, ranging from ionic and covalent bonding to host-guest and van der Waals stabilization.[27-30] These findings have broadened the scope of noble-gas chemistry and may also have implications for volatile storage and chemical evolution in planetary interiors.

† Corresponding author. E-mail: 2017054@xjit.edu.cn
† Corresponding author. E-mail: shicongding@jsnu.edu.cn
† Corresponding author. E-mail: jingmingShi@jsnu.edu.cn

Among the noble gases, xenon (Xe) is particularly prone to pressure-induced chemical activation because of its relatively low ionization energy and high polarizability. The conventional view of Xe as an inert element was first challenged by Pauling's prediction of xenon fluorides[31] and later overturned by the synthesis of Xe compounds with highly electronegative elements such as F and O under ambient conditions.[32,33] High pressure further enlarges the accessible chemical space of Xe. Xe-bearing compounds have been reported in systems containing H_2O, O_2, F, N, and S at relatively moderate pressures,[34-44] and in Fe-, Ni-, Mg-, oxide- and silicate-related systems at higher pressures.[45-47] These phases are of interest because they provide possible mechanisms for Xe retention in deep planetary reservoirs. In addition, Xe compounds with electropositive metals such as Li, Na, and K show that pressure can promote charge transfer to Xe and stabilize unusual noble-gas-rich stoichiometries.[48-52] These studies indicate that Xe chemistry under pressure is governed not only by structural confinement, but also by pressure-induced electronic redistribution, motivating the search for Xe-bearing phases in other systems.

Calcium is a major lithophile element in terrestrial planets and rocky super-Earths, and is widely hosted in crustal and mantle minerals. Its abundance, mineralogical hosts, and isotopic signatures provide important constraints on crust-mantle differentiation, deep material cycling, and planetary evolution.[53] Under high-pressure conditions, Ca-bearing compounds can adopt diverse structures and bonding environments, making calcium an important element for exploring pressure-induced chemical reactivity in planetary interiors. In our previous first-principles study, we predicted four stable Ca-Xe compounds, CaXe, $CaXe_2$, Ca_3Xe, and Ca_2Xe_3, within the 0-150 GPa pressure range. [54] These compounds are metallic and dynamically stable over broad pressure intervals. However, the Xe-rich region of the Ca-Xe system remains largely unexplored. Compared with the previously reported compounds, $CaXe_3$ contains a higher proportion of Xe, with Xe accounting for approximately 90.8 wt% of the compound. It therefore provides an opportunity to examine whether calcium can stabilize more Xe-rich compositions under pressures beyond the previously investigated range. This question is particularly relevant to rocky super-Earths, whose deep interiors can reach pressures far beyond those of Earth's mantle.[55]

In this work, we combine the swarm-intelligence-based CALYPSO structure prediction method with first-principles calculations to investigate the Ca-Xe system at 170 GPa, 200 GPa, 250 GPa and 300 GPa. Thermodynamic stability analysis identifies a previously unreported stable stoichiometry, $CaXe_3$. Electronic band-structure and density-of-states calculations show that $CaXe_3$ is metallic. Electron localization function (ELF) and Bader charge analyses further indicate that the Ca-Xe interaction is predominantly ionic, driven by pressure-enhanced charge transfer from Ca to Xe, which weakens the closed-shell stability of Xe and facilitates compound formation. In addition, ab initio molecular dynamics simulations show that $CaXe_3$ retains solid-like characteristics over a broad pressure-temperature range, suggesting that Xe effectively suppresses Ca diffusion under these conditions. These results establish the stability and bonding characteristics of the Ca-Xe system under high

pressure and identify a Ca-bearing Xe host phase that may be relevant to Xe sequestration in deep planetary interiors.

2. Computational details

We employed an automatic crystal structure search method based on the particle-swarm optimization algorithm implemented in the CALYPSO code to identify energetically favorable structures.[56-59] This method has been successfully applied to crystal structure prediction for a wide range of systems.[60-65] To search for stable Ca-Xe compounds, structure searches for Ca_xXe_y (x=1-3, y=1-3) were performed, with simulation cells containing up to four formula units. First-principles calculations, including structural optimizations and electronic-structure calculations, were performed within the framework of density functional theory (DFT) using the Vienna *Ab*-initio Simulation Package (VASP).[66,67] The exchange-correlation energy was described using the Perdew-Burke-Ernzerhof (PBE) functional within the generalized gradient approximation (GGA). The interactions between the valence electrons and ionic cores were treated using the projector-augmented wave (PAW) method, with $3p^6 4s^2$, and $5s^2 5p^6$ electrons treated as valence electrons for Ca and Xe, respectively. After convergence tests, the plane-wave cutoff energy of 1000 eV and k-point mesh of $2\pi \times 0.03$ Å^{-1} were set to ensure total energy and forces convergence better than 1 meV/atom and 1 meV/Å, respectively. Phonon calculations were carried out using a finite displacement method as implemented in PHONOPY code.[68,69] Ab initio molecular dynamics (AIMD) simulations were performed to investigate the dynamical behavior of $CaXe_3$ under high-pressure and high-temperature conditions. A 3 × 3 × 3 supercell containing 108 atoms was used for $P4/mmm$-$CaXe_3$, whereas a 2 × 2 × 2 supercell containing 128 atoms was used for $C2/m$-$CaXe_3$. The simulations were carried out in the canonical (NVT) ensemble using a Nosé-Hoover thermostat. Each simulation consisted of 10,000 time steps with a time step of 1 fs, corresponding to a total simulation time of 10 ps.[70] Crystal structures and electron localization functions ELFs were plotted using VESTA software.[71]

3. Results and discussion

To explore stable compounds in the Ca-Xe system under high pressure, we performed crystal-structure searches using the CALYPSO method over the pressure range of 170 GPa, 200 GPa, 250 GPa, and 300 GPa. The formation enthalpy per atom of each candidate compound was evaluated with respect to the elemental solid phases of Ca and Xe at the same pressure,

$$\Delta H = [H(Ca_xXe_y) - xH(Ca) - yH(Xe)]/(x+y) \quad (1)$$

where $H(Ca_xXe_y)$, H(Ca), and H(Xe) denote the enthalpies of the compound and the elemental reference phases, respectively. Based on these formation enthalpies, pressure-dependent convex-hull diagrams were constructed, as shown in Fig. 1(a) and Fig. S1. Compositions lying on the convex hull are thermodynamically stable against decomposition into the elemental phases or competing Ca-Xe compounds at the corresponding pressure. The calculated convex hulls show that $CaXe_3$ is thermodynamically stable at 170 GPa, 200 GPa, and 250 GPa [Fig. 1 and Fig. S1], whereas it becomes unstable at 300 GPa. Further pressure-dependent formation-enthalpy calculations indicate a stability range of approximately 170-290

GPa. Within this range, $CaXe_3$ adopts a tetragonal *P*4/*mmm* structure at lower pressures and transforms into a monoclinic *C*2/*m* phase near 220 GPa. In contrast, CaXe, Ca_2Xe_3, and $CaXe_2$ remain on the convex hull over the investigated pressure range, without undergoing structural phase transitions. The corresponding pressure-composition phase diagram of the Ca-Xe system is summarized in Fig. 1(d). The results indicate that $CaXe_3$ is stable within a finite pressure window of ~170-290 GPa. Therefore, the following discussion focuses on $CaXe_3$, as it is the newly identified phase in this work, whereas the other compounds are consistent with previously reported structures.[54]

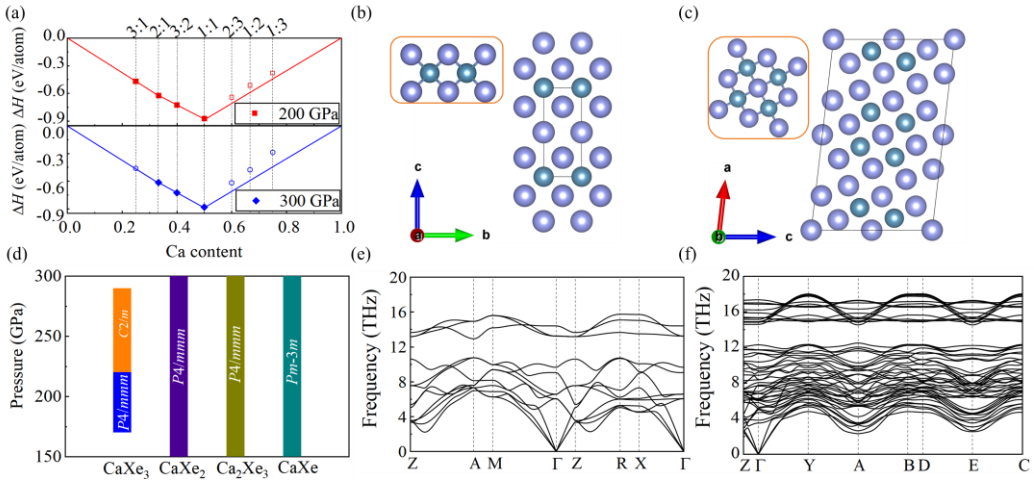


Fig. 1. (a) Convex hull of Ca_xXe_y compounds at 200 GPa and 300 GPa. Solid diamonds and circles denote stable structures, whereas open symbols denote unstable structures. Crystal structures of (b) *P*4/*mmm* at 170 GPa, and (c) *C*2/*m* at 220 GPa. (d) Pressure-composition phase diagram of the Ca-Xe system. Phonon dispersion curves of (e) *P*4/*mmm* at 170 GPa, and (f) *C*2/*m* at 220 GPa.

At 170 GPa, $CaXe_3$ adopts a tetragonal structure with space group *P*4/*mmm*, as shown in Fig. 1(b). Ca and Xe2 occupy the high-symmetry 1*a* and 1*b* Wyckoff sites, respectively, whereas Xe1 occupies the 2*h* site (Table S1 of the Supplemental Material).[72] The two symmetry-equivalent Xe1 atomic layers derived from the 2*h* positions lie between the alternating Ca and Xe2 layers, giving rise to a Ca-Xe1-Xe2-Xe1 stacking sequence along the *c* direction. The shortest Xe-Xe contact is 2.88 Å, while the nearest Ca-Xe and Ca-Ca distances are 2.56 Å and 2.95 Å, respectively. Upon further compression, $CaXe_3$ undergoes a structural transition from the tetragonal *P*4/*mmm* phase to a monoclinic *C*2/*m* phase at ~220 GPa, as shown in Fig. S2. The transition is accompanied by a lowering of crystal symmetry and a distortion of the Xe framework, leading to a more compact packing arrangement. As displayed in Fig. 1(c), the *C*2/*m* phase also exhibits a layered structural motif, in which Ca atoms are ordered within the interstitial regions of the Xe framework. The shortest Ca-Xe, Xe-Xe, and Ca-Ca distances in this phase are 2.49 Å, 2.78 Å, and 2.92 Å, respectively. Compared with the *P*4/*mmm* phase, the reduced Xe-Xe and Ca-Xe separations indicate enhanced compression of the Xe framework and enhanced Ca-Xe interactions at higher pressure. This pressure-induced structural contraction provides a useful basis for comparison with the related Xe_3K system. Interestingly, Xe_3K exhibits a similar *P*4/*mmm*-to-*C*2/*m* structural transition to $CaXe_3$. In

*C*2/*m*-Xe_3K, the Xe-K distances are 2.73-2.76 Å, and the positive Laplacian values of approximately 1.41-1.42 e $Å^{-5}$. [51] K transfers ~0.37 *e* to the Xe framework in *C*2/*m*-Xe_3K, while Ca transfers ~0.41 *e* in *C*2/*m*-$CaXe_3$. $CaXe_3$ shows stronger charge differentiation among inequivalent Xe sites, whereas the charge transfer in Xe_3K is more uniformly distributed. Thus, the comparable charge transfer and similar closed-shell metal-Xe interactions, despite the different nominal valence-electron counts of K and Ca, suggest that pressure-driven rearrangement of the Xe framework plays an important role in the *P*4/*mmm*-to-*C*2/*m* transition, beyond the effect of simple electron counting.[51] Figures 1(e) and 1(f) show the calculated phonon dispersion spectra of the *P*4/*mmm* or *C*2/*m* phases of $CaXe_3$, respectively. The absence of imaginary phonon modes throughout the Brillouin zone confirms the dynamical stability of both phases.

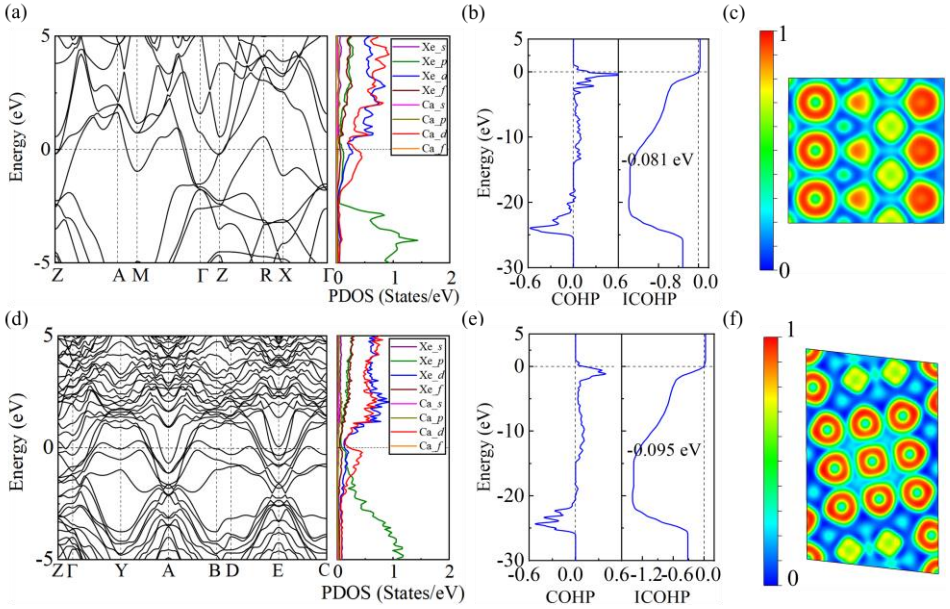


Fig. 2. Band structures and PDOS, crystal orbital Hamilton population (COHP) and integrated COHP (ICOHP), and electron localization function (ELF) maps for (a-c) *P*4/*mmm*-$CaXe_3$ at 170 GPa and (d-f) *C*2/*m*-$CaXe_3$ at 220 GPa, respectively.

Figures 2(a) and 2(d) show the electronic band structures and projected densities of states (PDOS) of the *P*4/*mmm* and *C*2/*m* phases, respectively. In both structures, bands cross the Fermi level, accompanied by an appreciable DOS at E_F, confirming the metallic character of $CaXe_3$. The occupied states below the E_F are dominated by Xe *p* orbitals, whereas Xe *d* and Ca *d* states contribute appreciably near the E_F. Notably, a non-negligible Xe *f* contribution is also present in the occupied states, although it is smaller than the Xe *p*, Xe *d* and Ca *d* contributions. In the *C*2/*m* phase, the Xe *d*- and *f*-projected states immediately below E_F exhibit peak profiles similar to those of the Ca *d* states. This correspondence suggests orbital hybridization among these states and is consistent with Ca-assisted activation of Xe *f* character under compression.

To clarify the nature of the Ca-Xe interactions, we performed Bader charge, quantum theory of atoms in molecules (QTAIM), integrated crystal orbital Hamiltonian population (ICOHP), and electron localization function (ELF) analysis.

The Bader analysis reveals charge transfers from each Ca atom to the Xe sublattice of ~0.499*e* in the *P*4/*mmm* phase and ~0.399-0.415*e* in the *C*2/*m* phase, indicating a substantial ionic contribution to Ca-Xe bonding (Table S2). The QTAIM analysis further identifies bond critical points between neighboring Ca and Xe atoms. At 170 GPa for *P*4/*mmm* and 220 GPa for *C*2/*m*, the electron-density Laplacians at these points are positive, with values of 4.897 and 2.860 e Å^{-5}, respectively (Table S3). These positive values are characteristic of closed-shell interactions rather than strong shared-shell covalent bonding. In addition, the Ca-Xe ICOHP values are -0.081 and -0.095 eV/pair for the *P*4/*mmm* and *C*2/*m* phases, respectively [Figs. 2(b) and 2(e)], indicating relatively weak Ca-Xe bonding interactions in both phases. Their small magnitudes are comparable to, but slightly smaller than, the reported Na-Cl ICOHP value of -0.13 eV/pair in ionic NaCl, further supporting the ionic nature of the Ca-Xe bonds. The ELF maps are consistent with these results, showing no appreciable electron localization in the Ca-Xe internuclear regions [Figs. 2(c) and 2(f)]. These complementary analyses confirm the formation of ionic Ca-Xe bonds in both phases.

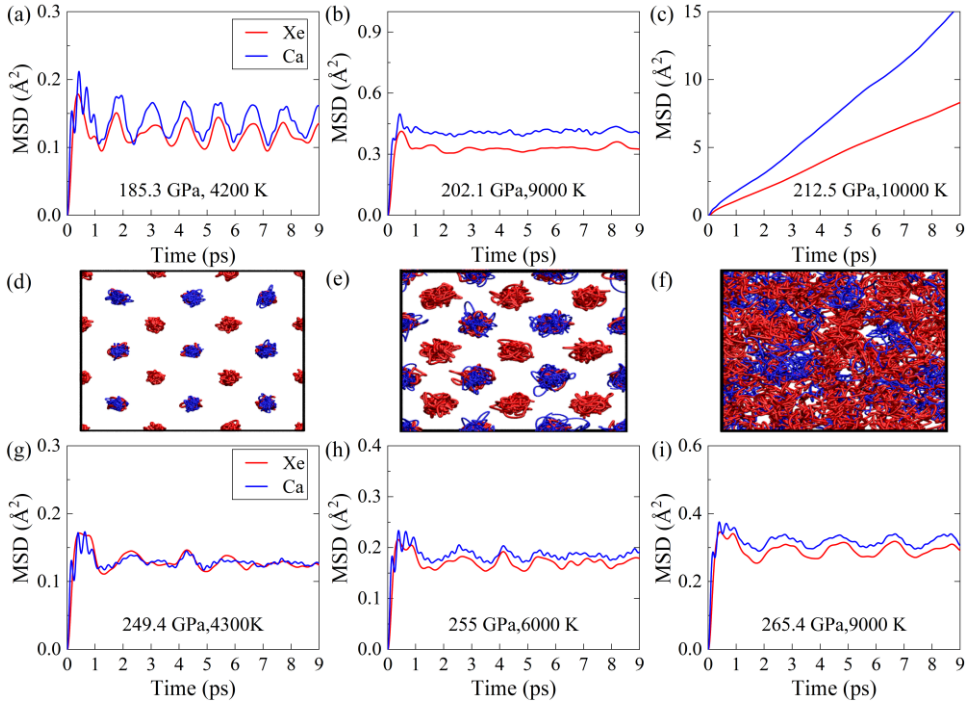


Fig. 3. (a-c) MSDs and (d-f) atomic trajectories during the final 9 ps of AIMD simulations of *P*4/*mmm*-$CaXe_3$ at different pressures and temperatures. (g-i) MSDs of *C*2/*m*-$CaXe_3$ at different pressures and temperatures. Blue and red trajectories represent Ca and Xe atoms, respectively.

The 170-290 GPa stability range of $CaXe_3$ extends into the pressure regime relevant to the core-mantle boundaries of rocky super-Earths,[55] where it may exist as a stable Xe-bearing compound. To further evaluate the relative thermodynamic stability of the two $CaXe_3$ phases at finite temperatures, we calculated their Gibbs free energies at 200, 230, and 250 GPa over the temperature range of 0–5000 K by combining static DFT energies with vibrational free energies obtained from phonon calculations within the quasiharmonic approximation [Fig. S3]. At 200 GPa, *P*4/*mmm*-$CaXe_3$ has a lower Gibbs free energy throughout the investigated temperature range, consistent with the static enthalpy ordering. At 230 and 250 GPa,

however, *C*2/*m*- $CaXe_3$ is thermodynamically favored at lower temperatures, whereas *P*4/*mmm*-$CaXe_3$ becomes stabilized at higher temperatures because of its larger vibrational entropy.

To probe its dynamical stability, we performed AIMD simulations in the canonical (*NVT*) ensemble over 170-290 GPa and temperatures up to 10,000 K. The atomic dynamics were characterized using the mean-square displacements (MSDs) and trajectories of Ca and Xe atoms. Based on the atomic diffusion behavior, $CaXe_3$ was classified into solid-like and liquid-like states. The calculated MSDs and atomic trajectories of the *P*4/*mmm*-$CaXe_3$ at different pressures and temperatures are depicted in Fig. 3(a)-(f). It is obvious that all the atoms in the *P*4/*mmm*-$CaXe_3$ vibrate at their equilibrium positions with diffusion coefficients of zero at 185.3 GPa and 4200 K [Fig. 3(a) and 3(d)]. This reveals that the *P*4/*mmm*-$CaXe_3$ phase exhibits a solid state at this condition. As pressure and temperature increase, the *P*4/*mmm*-$CaXe_3$ phase retains its solid character with all atoms not diffusive even at 202.1 GPa and 9000 K [Fig. 3(b) and 3(e)]. At 212.5 GPa and 10,000 K, by contrast, the MSDs increase continuously and the atomic trajectories become spatially extended, indicating liquid-like diffusion [Figs. 3(c) and 3(f)]. Under the investigated conditions below 10,000 K, the diffusion coefficients are effectively zero, corresponding to nearly zero MSD slopes and indicating solid-like behavior. At 10,000 K, the diffusion coefficients of Ca and Xe are 2.6×10^{-5} cm^2/s and 1.6×10^{-5} cm^2/s, respectively, demonstrating appreciable atomic diffusion and confirming the transition to a liquid-like state In contrast, *C*2/*m*-$CaXe_3$ consistently exhibits nearly zero MSD slopes at all investigated pressure–temperature conditions, indicating that it remains solid-like throughout the studied range [Fig. 3(g–i)]. Additional simulations at other temperatures show consistent trends [Fig. S5]. This indicates that $CaXe_3$ remains in a solid state under the extreme conditions of the lower mantle of rocky super-Earths. This is mainly caused by the strong ionic Ca-Xe bond, making the Ca-Xe configuration difficult to destroy. This research finding aligns with previous molecular dynamics simulations of KXe_3 and $NaXe_3$.[48-51]

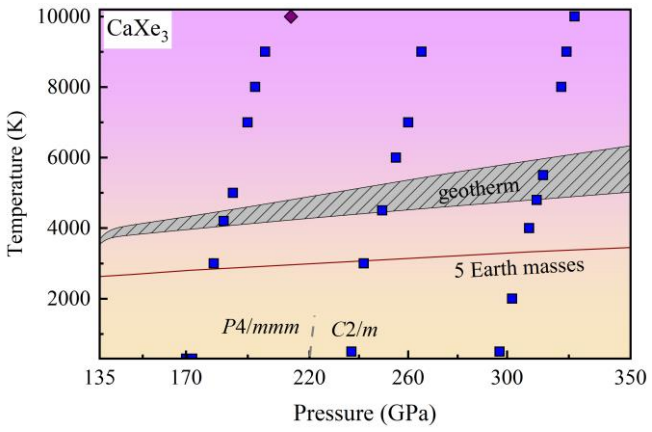


Fig. 4. The P-T phase diagram of $CaXe_3$ under the extreme conditions. The blue squares represent solid $CaXe_3$, while the purple rhombus represent molten $CaXe_3$, respectively. The gray shaded region represents Earth's geotherm, whereas the red line indicate the P-T conditions expected in the interiors of 5 times that of the Earth (M_E) rocky exoplanets.

Using these AIMD results, we constructed the P-T phase diagram of $CaXe_3$ shown in Fig. 4. The gray dashed lines delineate the structural stability fields of the low-pressure *P*4/*mmm* and high-pressure *C*2/*m* phases. As summarized in Fig. 4, $CaXe_3$ remains non-diffusive over most of the investigated P-T range, retaining solid-like behavior up to 9000 K. Liquid-like diffusion emerges only at 10,000 K, demonstrating its high thermal stability under extreme conditions. The thermodynamic stability range of $CaXe_3$, 170-290 GPa, extends into the core-mantle-boundary pressure regime predicted for $5M_E$ super-Earths, approximately 200-630 GPa.[55,73] Together, its broad pressure stability and high-temperature persistence identify $CaXe_3$ as a viable Xe-bearing phase in the deep interiors of rocky super-Earths.

At all sampled P-T points along the modeled geotherms of Earth and $5M_E$ rocky exoplanets, $CaXe_3$ retains solid-like behavior. Beyond its implications for super-Earth interiors, the predicted stability of $CaXe_3$ provides a concrete compound-level pathway relevant to the terrestrial missing-Xe problem. Although Ca is generally regarded as a lithophile element, high-pressure metal-silicate partitioning experiments and planetary accretion models suggest that trace-to-minor amounts of Ca may enter Earth's core during core formation, with modeled abundances below 1 wt%.[74] The 1:3 Ca:Xe stoichiometry of $CaXe_3$ allows each Ca atom to accommodate three Xe atoms, giving even a limited core Ca inventory substantial capacity for Xe sequestration. $CaXe_3$ therefore emerges as a candidate reservoir phase for the missing Xe in Earth's core and, more generally, as a high-pressure Xe-sequestration pathway in rocky exoplanets.

To further assess the possible relevance of $CaXe_3$ to deep planetary interiors, we calculated its density from the optimized structures, (Table S4). The densities of *P*4/*mmm*-$CaXe_3$ are 11.89 and 12.47 g/cm^3 at 170 and 200 GPa, respectively, while those of *C*2/*m*-$CaXe_3$ are 12.85 and 13.97 g/cm^3 at 220 and 290 GPa, respectively. These values are substantially higher than those of $MgSiO_3$ under comparable pressure conditions (approximately 5.7-6.5 g/cm^3),[75] a representative silicate component of deep planetary mantles, and are comparable to the densities of metallic core liquids such as liquid Fe at high pressures (9-12 g/cm^3).[76] The high density of $CaXe_3$, together with its high-pressure stability and high-temperature solid-like behavior, provides an additional quantitative constraint supporting its possible compatibility with dense regions of deep super-Earth interiors. Nevertheless, its actual role in planetary Xe sequestration will depend on the availability of Ca and the relative stability of $CaXe_3$ with respect to competing phases in realistic multicomponent planetary compositions.

4. **Conclusions**

In summary, we identify a previously unreported Xe-rich compound, $CaXe_3$, stable from 170 to 290 GPa, with a *P*4/*mmm*-to-*C*2/*m* transition near 220 GPa. Both phases are metallic and dynamically stable, with ionic Ca-Xe bonding arising from pressure-induced Ca-to-Xe charge transfer. AIMD simulations show that $CaXe_3$ remains solid-like up to 9000 K, whereas liquid-like diffusion emerges at 10,000 K.

Its P-T stability and 1:3 Ca:Xe stoichiometry identify $CaXe_3$ as a candidate Xe host in Earth's core and rocky super-Earth interiors, providing a possible compound-level route for Xe sequestration. These findings broaden the understanding of high-pressure Xe chemistry and provide a new chemical basis for modeling Xe sequestration in planetary interiors.

Acknowledgment

The authors acknowledge financial support from the Natural Science Foundation of Xinjiang Uygur Autonomous Region under Grant No. 2023D01C220 and the National Natural Science Foundation of China (NSFC) under Grant Nos. 12664006 12474123, 12574064, 12604024, 12174160, and 12074154. Y.L. acknowledges funding from the Six Talent Peaks Project. Y.L. and J.S. acknowledge funding from the 333 High-level Talents Project of Jiangsu Province. Y.L. acknowledges Jiangsu Normal University high-quality science and technology cultivation Project under grant Nos. JSNUGZL2026094.

References

[1] Xu M, Li Y and Ma Y 2022 *Chem. Sci*. 13 329-344
[2] Zhang L, Wang Y, Lv J and Ma Y 2017 *Nat. Rev. Mater.* 2 17005
[3] Miao M, Sun Y, Zurek E and Lin H 2020 *Nat. Rev. Chem*. 508-527
[4] Dong X, Oganov A R, Goncharov A F, Stavrou E, Lobanov S, Saleh G, Qian G-R, Zhu Q, Gatti C, Deringer V L et al. 2017 *Nat. Chem.* 9 440-445
[5] Gao X, Wei S, Guo Y, Yin G, Meng Y, Ju X, Chang Q and Sun Y 2024 *J. Phys.: Condens. Matter* 36 095402
[6] Liu X, Wei S, Gao X, Guo Y, Liu S, Ju X, Chang Q and Sun Y 2025 *Comput. Mater. Sci.* 248 113597
[7] Cao Y, Song H, Yan X, Wang H, Wang Y, Wu F, Zhang L, Wu Q and Geng H 2024 *Phys. Chem. Chem. Phys*. 26 19228-19235
[8] Takezawa H, Hsu H, Hirose K, Sakai F, Fu S, Gomi H, Miwa S and Sakamoto N 2025 *Phys. Rev. Lett.* 134 084101
[9] Huang Y S, Song H X, Hao Q D, Pan X L, Wang D, Wang H, Wang Y F, Sun Y and Geng H Y 2024 *Phys. Rev. B* 110 214102
[10] Shi J, Cui W, Hao J, Xu M, Wang X and Li Y 2020 *Nat. Commun.* 11 3164
[11] Liu C, Gao H, Hermann A, Wang Y, Miao M, Pickard C J, Needs R J, Wang H-T, Xing D and Sun J 2020 *Phys. Rev. X* 10 021007
[12] Zhang P, Shi J, Cui W, Liu C, Ding S, Yang K, Hao J and Li Y 2022 *Phys. Rev. B* 105 214109
[13] Zhang P, Ding Y, Cui W, Hao J, Shi J and Li Y 2024 *J. Chem. Phys*. 161 014501
[14] Gao H, Liu C, Hermann A, Needs R J, Pickard C J, Wang H-T, Xing D and Sun J 2020 *Natl. Sci. Rev*. 7 1540-1547
[15] Liu H, Yao Y and Klug D D 2015 *Phys. Rev. B* 91 014102
[16] Kim M, Oka K, Ahmed S, Somayazulu M S, Meng Y and Yoo C-S 2022 *J. Phys.: Condens. Matter* 34 394001

[17] Liu C, Gao H, Wang Y, Needs R J, Pickard C J, Sun J, Wang H-T and Xing D 2019 *Nat. Phys.* 15 1065-1070
[18] Ding S, Zhang P, Yang K, Liu C, Hao J, Cui W, Shi J and Li Y 2022 *Phys. Rev. B* 106 024102
[19] Liu C, Wang J, Deng X, Wang X, Pickard C J, Helled R, Wu Z, Wang H-T, Xing D and Sun J 2022 *Chin. Phys. Lett.* 39 076101
[20] Zhang J, Lv J, Li H, Feng X, Lu C, Redfern S A, Liu H, Chen C and Ma Y 2018 *Phys. Rev. Lett.* 121 255703
[21] Yang K, Yang K, Yang T, He J, Yang M and Zhou T 2024 *Phys. Rev. B* 110 054108
[22] Zhu J, Bao K, Zhou C, Zhang Z, Yu H, Liu Y and Cui T 2024 *Phys. Rev. B* 110 094111
[23] Wang Y, Zhang J, Liu H and Yang G 2015 *Chin. Phys. Lett.* 32 046401
[24] Yan X Z, Chen Y M and Geng H Y 2019 *ACS Omega* 4 13640-13644
[25] Wang M, Kuzovnikov M A, Binns J, Li X, Peña-Alvarez M, Hermann A, Gregoryanz E and Howie R T 2023 *J. Chem. Phys.* 159 134508
[26] Liu C, Boronat J and Cazorla C 2026 *Phys. Rev. B* 113 054101
[27] Li Y, Feng X, Liu H, Hao J, Redfern S A, Lei W, Liu D and Ma Y 2018 *Nat. Commun*. 9 722
[28] Hou J, Weng X-J, Oganov A R, Shao X, Gao G, Dong X, Wang H-T, Tian Y and Zhou X-F 2021 *Phys. Rev. B* 103 L060102
[29] Hou J, Wang X, Zhu Q, Shao X, Qiu S, Weng X-J, Yang G, Dong X, Zhou X-F and Tian Y 2025 *J. Am. Chem. Soc*. 147 33453–33459
[30] Hou J, Zhu Q, Weng X-J, Shao X, Dong X, Wang H-T, Zhou X-F and Tian Y 2025 *Adv. Sci*. 12 2415517
[31] Bartlett N 1962 *Proc. Chem. Soc.* London 218
[32] Levy H A and Agron P 1963 *J. Am. Chem. Soc*. 85 241-242
[33] Templeton D H, Zalkin A, Forrester J and Williamson S M 1963 *J. Am. Chem. Soc.* 85 817-817
[34] Sanloup C, Bonev S A, Hochlaf M and Maynard-Casely H E 2013 *Phys. Rev. Lett.* 110 265501
[35] Hu K, Geng Y, Zhu K, Gu Y and Yu J 2024 *Phys. Lett. A* 514 129618
[36] Peng F, Botana J, Wang Y, Ma Y and Miao M 2016 *J. Phys. Chem. Lett.* 7 4562-4567
[37] Zhu Q, Jung D Y, Oganov A R, Glass C W, Gatti C and Lyakhov A O 2013 *Nat. Chem.* 5 61-65
[38] Hermann A and Schwerdtfeger P 2014 *J. Phys. Chem. Lett.* 5 4336-4342
[39] Dewaele A, Worth N, Pickard C J, Needs R J, Pascarelli S, Mathon O, Mezouar M and Irifune T 2016 *Nat. Chem.* 8 784-790
[40] Dewaele A, Loubeyre P, Dumas P and Mezouar M 2012 *Phys. Rev. B* 86 014103
[41] Somayazulu M, Dera P, Goncharov A F, Gramsch S A, Liermann P, Yang W, Liu Z, Mao H-k and Hemley R J 2010 *Nat. Chem.* 2 50-53
[42] Mao H and Hemley R 2001 *Proc. Natl. Acad. Sci*. 98 10513-10518
[43] Peng F, Wang Y, Wang H, Zhang Y and Ma Y 2015 *Phys. Rev. B* 92 094104

[44] Yan X, Chen Y, Xiang S, Kuang X, Bi Y and Chen H 2016 *Phys. Rev. B* 93 214112
[45] Zhu L, Liu H, Pickard C J, Zou G and Ma Y 2014 *Nat. Chem.* 6 644-648
[46] Peng F, Song X, Liu C, Li Q, Miao M, Chen C and Ma Y 2020 *Nat. Commun.* 11 5227
[47] Miao M-s, Wang X-l, Brgoch J, Spera F, Jackson M G, Kresse G and Lin H-q 2015 *J. Am. Chem. Soc.* 137 14122-14128
[48] Zou M, Yang K, Zhang P, Cui W, Hao J, Shi J and Li Y 2023 *Phys. Rev. Res*. 5 043107
[49] Peng J, Wang S, Dong H, Wen M, Zhang X and Wu F 2024 *Phys. Rev. B* 109 L140103
[50] Tian Y, Tse J S, Liu G and Liu H 2022 *Phys. Chem. Chem. Phys.* 24 18119-18123
[51] Lu C, Yang K, Cui W, Hao J, Shi J and Li Y 2024 *Phys. Rev. B* 110 024111
[52] Liu Z, Botana J, Miao M and Yan D 2017 *Europhys. Lett*. 117 26002
[53] Valencia D, Ikoma M, Guillot T and Nettelmann N 2010 *Astron. Astrophys*. 516 A20
[54] Zhang P, Cui W, Hao J, Shi J and Li Y 2025 *J. Chem. Phys.* 162 104502
[55] Unterborn C T and Panero W R 2019 *J. Geophys. Res.: Planets* 124 1704-1716
[56] Gao B, Gao P, Lu S, Lv J, Wang Y and Ma Y 2019 *Sci. Bull.* 64 301-309
[57] Wang Y, Lv J, Zhu L and Ma Y 2012 *Comput. Phys. Commun*. 183 2063-2070
[58] Wang Y, Lv J, Zhu L and Ma Y 2010 *Phys. Rev. B* 82 094116
[59] Shao X, Lv J, Liu P, Shao S, Gao P, Liu H, Wang Y and Ma Y 2022 *J. Chem. Phys.* 156 014105
[60] Li Y, Wang Y, Pickard C J, Needs R J, Wang Y and Ma Y 2015 *Phys. Rev. Lett*. 114 125501
[61] Gao K, Cui W, Chen J, Wang Q, Hao J, Shi J, Liu C, Botti S, Marques M A and Li Y 2021 *Phys. Rev. B* 104 214511
[62] Wang Q, Cui W, Gao K, Chen J, Gu T, Liu M, Hao J, Shi J and Li Y 2022 *Phys. Rev. B* 106 054519
[63] Xu M, Huang C, Li Y, Liu S, Zhong X, Jena P, Kan E and Wang Y 2020 *Phys. Rev. Lett.* 124 067602
[64] Cui W, Bi T, Shi J, Li Y, Liu H, Zurek E and Hemley R J 2020 *Phys. Rev. B* 101 134504
[65] Shi J, Cui W, Botti S and Marques M A 2018 *Phys. Rev. Mater.* 2 023604
[66] Kresse G and Furthmüller J 1996 *Phys. Rev. B* 54 11169
[67] dos Santos A V, Padilha G and Monçalves M 2012 *Solid State Sci.* 14 269-275
[68] Parlinski K, Li Z and Kawazoe Y 1997 *Phys. Rev. Lett.* 78 4063
[69] Togo A, Oba F and Tanaka I 2008 *Phys. Rev. B* 78 134106
[70] Hoover W G 1985 *Phys. Rev. A* 31 1695
[71] Momma K and Izumi F 2011 *J. Appl. Crystallogr.* 44 1272-1276
[72] See Supplemental Material at [URL will be inserted by publisher], It contains structural configurations and parameters, Bader charge, phonon dispersion, band structures, ELFs and DOS of the predicted $CaXe_3$ compounds at different pressures.
[73] Rajkrishna Dutta, Sally J. Tracy, and R. E. Cohen 2023 *Phys. Rev. B* 107 184112

[74] Chidester B A, Lock S J, Swadba K E, Rahman Z, Righter K and Campbell A J 2022 *Geochem. Geophys. Geosyst.* 23 e2021GC009986
[75] Wagle F and Steinle-Neumann G 2019 J. Geophys. Res. Solid Earth 124 3350
[76] Bolis R M, Morard G, Vinci T, Ravasio A, Bambrink E, Guarguaglini M, Koenig M, Musella R, Soubiran F, Hernandez J A, Caracas R and Bouchet J 2021 Nat. Commun. 12 789